IOP Conf. Series: Earth and Environmental Science **1487** (2025) 012191 doi:10.1088/1755-1315/1487/1/012191

Prediction of Water Storage Volume in Soil Surface Layers Using Geomatics Techniques

Forqan Kh. Al-Daraji[1], Najed Faisal Shareef[2] and Wisam B. Hasan[3]

[1,2]Department of Applied Marine Sciences, College of Marine Sciences, University of Basrah, Basrah, Iraq.
[3]Department of Project Management, College of Administration and Economics Qurna, University of Basrah, Basrah, Iraq.

[1]E-mail: forqan.khalid@uobasrah.edu.iq
[2]E-mail: najid.shareef@uobasrah.edu.iq
[3]E-mail: wisam.hasan@uobasrah.edu.iq

Abstract. This study was conducted in the northeastern area of the left bank of Shatt al-Arab left riverside north of Basrah Governorate of Iraq. Suitable satellite imagery for the study area was collected in July 13, 2023 coinciding with the time of field sample collection. The selected imagery underwent spectral correction followed by classification of the study area to identify and distribute sample collection sites evenly across three locations. Field samples were collected from the soil surface layers to calculate the volume of water stored in the soil. A predictive model was developed to relate the volumetric soil moisture index derived from the thermal difference of the land surface. Soil moisture content was modelled and predicted using remote sensing data and a balancing algorithm. The volumetric soil moisture values (%PW) were derived based on the Soil Moisture Index (SMI) representing the thermal difference of the land surface, calculated from thermal equations of LST values. The study concluded that the proposed predictive model effectively monitors and estimates the volume of water stored in the soil demonstrating the potential of using remote sensing data and satellite imagery in water resource studies. It was found that areas far from water sources with sparse vegetation experience higher temperatures leading to increased water deficit in the study area. Additionally, there is an increase in the volume of water stored in the soil in areas near water sources, due to the impact of lateral water feeding from Shatt al-Arab River and its tributaries towards the adjacent soils.

Keywords. Water resource management, Soil Moisture, Water balance, Semi-arid, Soil Water stored.

1. Introduction

Stored water in the surface layers of soil is a crucial factor for water balance, directly affecting ecosystem stability and sustainability. It is a vital resource for essential uses including human industrial and agricultural applications [1]. Estimating the volume quantity and distribution of water stored in the soil presents significant challenges for hydrologists and water resource managers particularly in the ecological context of Iraq and specifically in Basrah Governorate [2] .Mathematical and statistical models play an important role in predicting the volume of stored water and

understanding the factors influencing it [3]. Soil water storage refers to water present in soil pores, which can be either saturated or unsaturated. water moves horizontally and vertically under the influence of pressure differentials and hydraulic gradients between high and low-pressure areas[4] .This movement creates spatial variations in stored water, with higher levels near recharge sources and lower levels further away, This phenomenon directly impacts plant nutrition and crop growth, influencing temperature reduction and climate improvement in the region[5]. Stored water also affects the chemical, physical, and hydrological properties of soil This is reflected in the rise of groundwater levels near recharge sources potentially leading to soil degradation and alterations in its engineering properties. Therefore, it can be concluded that water stored in the surface layers of soil plays a significant role in achieving environmental and agricultural sustainability [6]. Used of remote sensing technologies to study the significance of environmental and climatic factors and their impact on the volume and distribution of soil water plays a crucial role in effective water resource management. To achieve the research objectives, the focus is on the following points.

- Utilizing Geomatics to Minimize Effort and Time: Geomatics technologies can significantly reduce the effort and time required for monitoring stored water or surface water resources. By leveraging these technologies, researchers can efficiently gather and analyze large-scale data, enhancing the accuracy and speed of water resource assessments.
- Monitoring Temporal and Spatial Variability: Remote sensing allows for the observation of temporal and spatial variations in stored soil water and the environmental factors influencing it. This capability is essential for understanding how water availability changes over time and space, and for identifying the factors that affect soil water distribution.

By integrating these approaches, the study aims to improve water resource management practices and contribute to more effective and sustainable use of water resources

2. Materials and Methods

2.1. Study Location

A study was conducted in the area located northeast of the left bank of the Shatt al-Arab River, extending from the Al-Suweib River towards Qada of Shatt al-Arab Island in Basrah government (Figure 1).

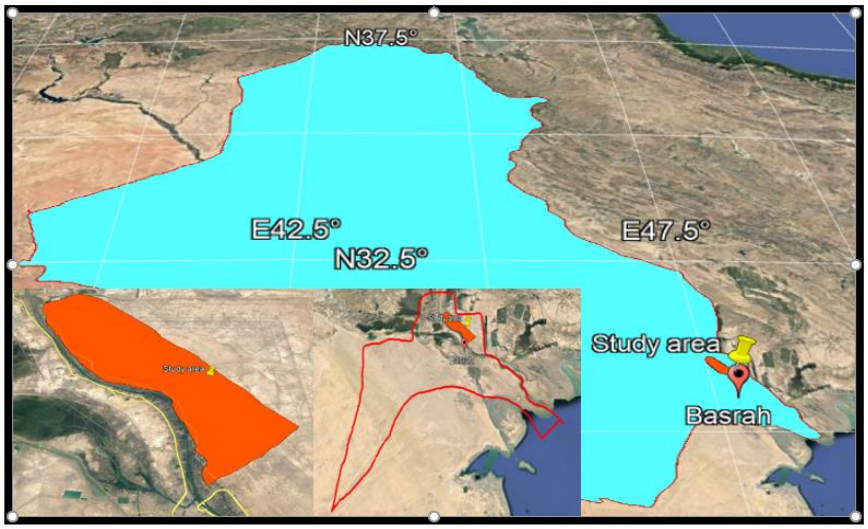

Figure 1. Study location.

2.2. Office Work

Satellite imagery suitable for the study area coinciding with the field sample collection date of July 13/ 2023 was collected. The imagery from the Landsat 8 satellite was obtained from the U.S. Geological Survey (USGS) website. Spectral correction was performed on the selected imagery followed by a

false-color classification of the study area to identify and evenly distribute three sample collection sites.

2.3. Field Work

Field samples were collected from the soil surface layers using a core sampler at depths of 0-30 cm and 30-45 cm, The samples were then weighed in their wet state and the following measurements were taken:

2.3.1. Measurement of Bulk Density, Particle Density and Total Porosity of Soil

Soil particle density, bulk density and porosity were estimated using the method described by [7]. Undisturbed soil samples were collected to estimate bulk density using a core sampler with a metal cylinder of dimensions 5 cm x 5 cm Bulk density was then calculated using the following equation:

$$\rho b = M_s / v \quad (1)$$

ρb is bulk density (g/cm³), Ms is dry soil mass (g) and V is the cylinder volume which equals the soil volume (cm³).

Soil particle density (ρ_s) was estimated using the pycnometer method, The total porosity (%S) was calculated based on the relationship between bulk density and particle density by applying the following equation:

$$S=1- (\rho b / \rho s) \times 100 \quad (2)$$

2.3.2. Soil Moisture Content

Soil samples were collected using a core sampler, then weighed immediately after collection. The samples were air-dried and placed in an oven at $105°_C$ until a constant weight was achieved. The dry weight and soil moisture content relative to its dry weight (Pw) were then calculated using the thermal gravimetric method described in[7] , as shown in the following equation:

$$Pw = ((Mm - Ms)) / Ms \quad (3)$$

PW: Soil moisture content (g water. g soil).
M_m: Mass of wet soil (g).
M_s: Mass of dry soil (g).

2.4. Predictive Models and Statistical Analysis

2.4.1. Land Surface Temperature

Field data for daily temperature values were collected from the Qurna Climate Station in Basrah Governorate, located at coordinates E 47°.45 and N 30°.94 which is part of the Agricultural Meteorological Center of the Iraqi Ministry of Agriculture, Values corresponding to the time of satellite imagery acquisition were used.

Land Surface Temperature (LST) calculations and modeling for the study area were performed using the thermal equilibrium algorithm. This involved deriving thermal energy values from the thermal infrared Band 10, the red infrared Band 4, and the near-infrared Band 5. Radiative energy in the upper atmosphere and thermal emissivity of the soil surface as well as the effect of vegetation cover were calculated LST values for each pixel with dimensions of 30×30 m or less depending on the spatial resolution of the satellite imagery were then determined. A comparison was made between the modeled values and those obtained from the ground-based climate station data and field temperature readings recorded at the same station, which measures temperatures over a limited area. The following equations can be used to calculate temperature values using satellite imagery data[8]:

- First: Calculate the spectral radiance from satellite imagery using the following equation:

$$L \lambda = M_L \times Q_{cal} + A_L - Oi \quad (4)$$

L (λ): is the Top-of-Atmosphere (TOA) spectral radiance.

M_L&$A_{L:}$ are constants for Band 10, which can be obtained from the metadata file accompanying the satellite imagery (MULT_BAND and ADD_BAND).
Band 10: refers to the thermal infrared band.
Oi :is calibration factor for Band 10 (0.29).

- Second: Convert the spectral radiance to brightness temperature in degrees Celsius using the following equation:

$$BT= (K2/ \ln (K1 / L\lambda+1) – 273.15 \quad (5)$$

L (λ) : is spectral radiance.
BT: is brightness temperature in degrees Celsius.
K2&K1: are constants for Band 10 from the metadata file.
273.15: is constant for converting temperature from Kelvin to Celsius.

- Third: Calculate the vegetation coverage portion using the following equation:

$$Pv= ((NDVI - NDVI\ min) / (NDVI\ max - NDVI\ min))^2 \quad (6)$$

PV: is the vegetation coverage.
NDVI: is the Normalized Difference Vegetation Index from imagery.
$NDVI_{max}$ and $NDVI_{min}$: are the maximum and minimum NDVI values from the imagery.

- Fourth: Calculate the land surface emissivity using the following equation:

$$E = 0.004 \times Pv + 0.98 \quad (7)$$

PV :is vegetation coverage.

- Fifth: Calculate the Land Surface Temperature (LST) using the following equation:

$$LST= BT / (1+(W\times BT/C2) \times \ln(E)) \quad (8)$$

LST :is land surface temperature in degrees Celsius.
BT: is brightness temperature in degrees Celsius.
E :is land surface emissivity.
W :is wavelength of Band 10 (10.8 μm).
C2 :is a constant calculated using the following equation:

$$p=h \times C/S = 1.4388 \times 10^{-2}\ mk = 14388\ \mu mk \quad (9)$$

S :is t constant Boltzmann (1.38×10^{-23}Joules per Kelvin).
h: is Planck's constant (6.626×10^{-34} Joules sec).
C :is the speed of light (2.998×10^{8} m/sec).

- Sixth: The correlation coefficient and coefficient of determination between the values calculated using satellite imagery and the field values from the climate station were computed using correlation analysis in SPSS, showing a significant correlation of 0.976.
- Seventh: A model was programmatically developed as a tool within the ARC GIS environment, as shown in the schematic diagram in Figure 2.

2.4.2. Volume of Water Stored in the Soil Profile

The amount of water stored in the soil was calculated by developing a predictive model based on the Soil Moisture Index derived from the land surface thermal difference, as shown in Equation (8). Soil moisture content was modeled and predicted using remote sensing data and the thermal balance algorithm as mentioned in [9]، Soil moisture values (PW%) were derived based on the Soil Moisture Index, which represents the land surface thermal difference as indicated in Equation (10), and is calculated from the thermal equations of LST values (Equation 10). It can be computed using the following equation:

$$Soil\ moisture\ index_{((SMC))} = ((LSTmax – LST) / (LSTmax – LSTmin)) \quad (10)$$

LST: As mentioned in Equation 8.
LSTmax: maximum recorded temperature value in study area.

LSTmin: minimum recorded temperature value in study area.

The values of the SMC index range from 0 to 1, where the soil is considered dry as the index approaches zero, and moisture increases as the values approach one. The index can reveal the presence of free water surfaces or saturated soil if the index values are greater than 1[10]. Regression analysis was then performed between the soil moisture index values and the field-measured bulk moisture values (PW) to obtain the constants of the predictive equation, which is expressed in its final form as follows:

$$\%PW=B \times ((LSTmax - LST) / (LSTmax - LSTmin))^2 + B \times ((LSTmax - LST) / (LSTmax - LSTmin))^3 - A \quad (11)$$

%Pw: Soil moisture content by mass estimated through remote sensing.

A+B: Constants from the equation in Table1.

((LSTmax – LST)/(LSTmax – LSTmin)): As mentioned in Equation (10)

The correlation coefficient and the coefficient of determination were calculated between the values obtained using satellite imagery and the field-measured values from the station using correlation analysis in SPSS. Subsequently, a software model was developed as a tool within the ARC GIS environment, as shown in the diagram below (Figure 3).

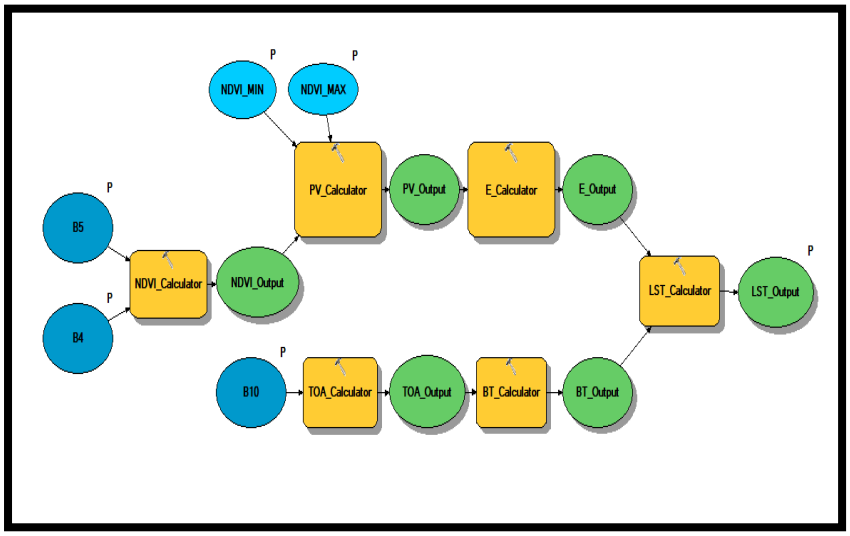

Figure 2. Steps for Using Thermal Balance Tool in ARC MAP.

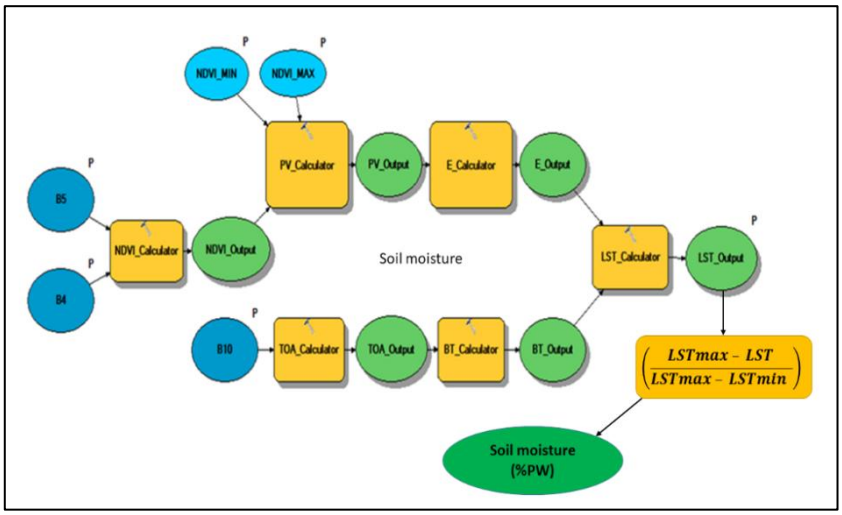

Figure 3. Steps for Running Thermal-Moisture Model in ARC MAP.

3. Results and Discussion

3.1. Land Surface Temperature (LST) in the Study Area

The results shown in Figure (4) illustrate the land surface temperature values measured using thermal algorithms and satellite imagery. There is a clear variation in temperature values within the study area, with a range from the lowest value of 34.85°C to the highest value of 50.84°C. Temperatures are higher in barren areas far from water sources and with sparse vegetation, while they are lower in most areas adjacent to the Shatt al-Arab River and its tributaries. Based on this spatial variation, the study area was divided into three categories. The lowest temperature category, with a range from 34.85 to 41.81°C, was found in the areas adjacent to the Shatt al-Arab River and most agricultural areas. In contrast, the highest temperature values, ranging from 47.65 to 50.84°C, were recorded in the remote and barren areas [11].

The thermal variation among the categories in the study area is a result of the clear differences in certain climatic, environmental, and natural and human activities such as land use, vegetation cover, and variation in soil moisture content, which are crucial for the exchange of energy and mass between the hydrosphere, atmosphere, and biosphere[12] . It is observed that the first category, representing most agricultural areas with vegetation and proximity to the banks of the Shatt al-Arab River and water sources, has the lowest temperature values compared to the second and third categories, which primarily represent urban and barren exposed areas. This is attributed to the impact of vegetation cover in absorbing some thermal radiation and carbon dioxide, as well as its large coverage area on the land surface, which improves air quality and reduces the greenhouse effect. Additionally, soil moisture content plays a key role in the thermal balance of the land surface due to the thermal capacity of water, which helps in dissipating thermal energy[13] .

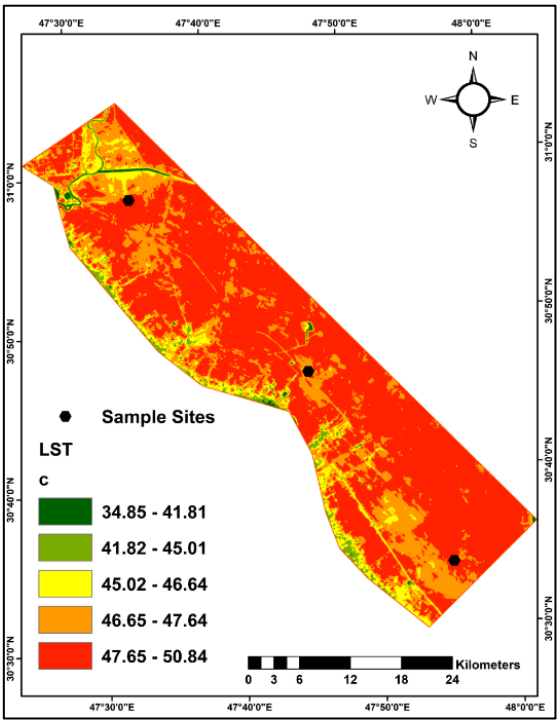

Figure 4. Spatial Distribution of Land Surface Temperature (LST) from Remote Sensing.

3.2. Surface Soil Moisture Index in the Study Area

The results shown in Figure (5) display the Soil Moisture Index values for the months of January, April, July, and October in the study area. Generally, there is spatial variation in the values, which is attributed to changes in some hydro-physical and climatic properties of the soil. The index values range from 0 to 1, with soil considered dry as the index approaches zero and increasing moisture as the values approach one[14] .

The Soil Moisture Index values for the second category showed the highest spatial distribution at 52.34%, while the values for the first and second categories were similar in percentage distribution within the study area, at 22.31% and 20.08%, respectively. The fourth category recorded the lowest spatial distribution compared to the other three categories, at 2.88%. This is attributed to the stability of the thermal signature curve for land phenomena such as water, vegetation cover, barren soil, and its moisture. Additionally, the inverse relationship between vegetation cover and soil moisture with land surface temperature plays a role, where higher vegetation index and soil moisture content lead to lower surface temperatures. This, in turn, reduces the processes of evaporation and evapotranspiration and enhances the soil's ability to retain water [9].

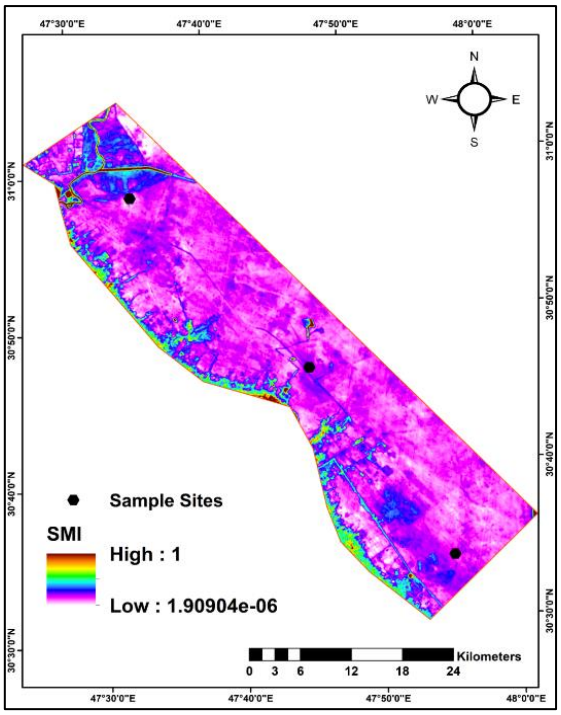

Figure 5. Spatial Distribution of Soil Moisture Index from Remote Sensing.

3.3. Evaluation of Predictive Model

Results shown in Table 1 and Figure (6) indicate a significant positive correlation between field moisture values (%PW) and the values predicted using remote sensing. The highest correlation coefficient (r) recorded was 0.84 for the month of July. This high correlation is attributed to the reduced cloud cover and its effect on the scattering and absorption of electromagnetic energy reaching the Earth's surface in July. [15].

This helps increase the spectral accuracy of the thermal band 10 with a wavelength of 10.60 - 11.19 micrometers. These results are consistent with those found in[16] , where they identified a highly significant positive correlation of 0.81 and 0.83 between soil moisture content and the Soil Moisture Index (SMI) calculated from remote sensing data for the thermal band 10 of Landsat-8 satellites, respectively. The thermal data also showed good results for predicting soil moisture content and distribution, as compared to 100 field samples collected from various sites in arid and semi-arid regions at a depth of 0-10 cm.

Table 1. Statistical Properties and Constants of Predictive Equations.

Model Summary between independent variable is SMI and FMC		
R	**R Square**	**Type of Regression**
0.847	0.718	Cubic
Coefficients		
Standardized Coefficients	Unstandardized Coefficients	
B (SMI^2)	-3378.293	

Model Summary between independent variable is SMI and FMC					
R	**R Square**		**Type of Regression**		
C (SMI^3)			13193.729		
A (Constant)			34.607		
	ANOVA Table				
S.O.V	Sum of Squares	df	Mean Square	F	Sig.
Regression	11.707	2	5.853	1.969	0.394
Residual	0.36	1			
Total	11.707	2			
The independent variable is SMI.					

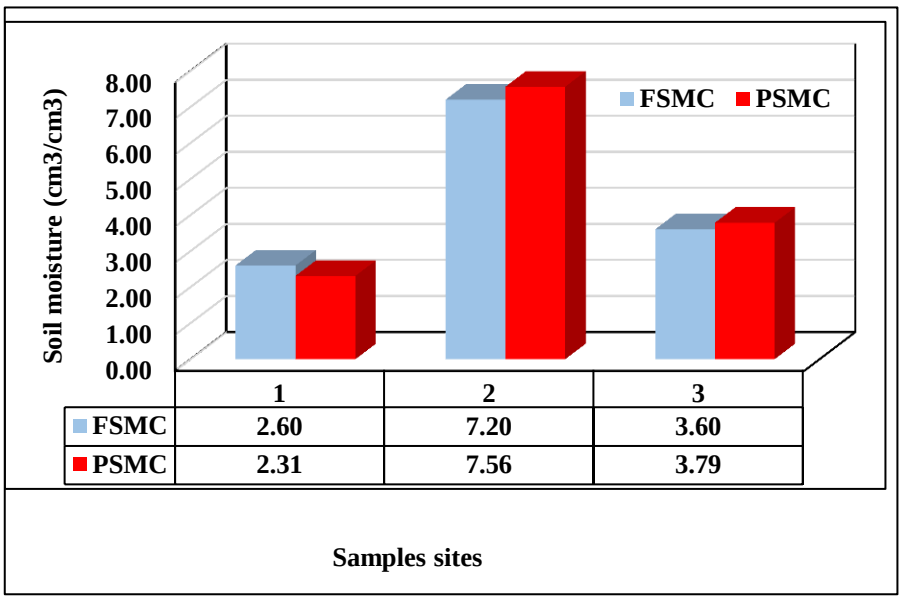

Figure 6. Comparison of Remote-Sensing Soil Moisture with Field Measurements.

3.4. Modeling Soil Moisture Using Remote Sensing

The results shown in Figures (7) and (8) reveal a clear spatial variation in soil moisture content and the volume of water stored in the soil within the study area. Regarding the spatial variation of soil moisture content, areas with good vegetation cover, especially agricultural areas along the banks of the Shatt al-Arab River, recorded moisture values ranging from 4% to 11%. This was followed by most barren areas far from water sources, which recorded the lowest moisture range of 0.0% to 0.88%. Other categories showed a range between the highest and lowest values, representing sites with irrigation canal branches near the Shatt al-Arab River, covering an area of 12.73%, as well as small areas within the barren regions. This variation may be attributed to the higher depth of groundwater in areas adjacent to rivers and irrigation canals due to lateral seepage and water replenishment through the soil, which leads to an increase in soil moisture content[17]. variation in soil moisture content in the study area can be attributed to several factors, the most significant of which is the variation in evapotranspiration rates due to differences in temperatures throughout the seasons (Figure 3) and its impact on the water balance in the region. High temperatures, reduced vegetation cover, and extensive barren areas, particularly in the summer, lead to decreased soil moisture content due to the rapid loss of water particles through evaporation and transpiration processes [18].

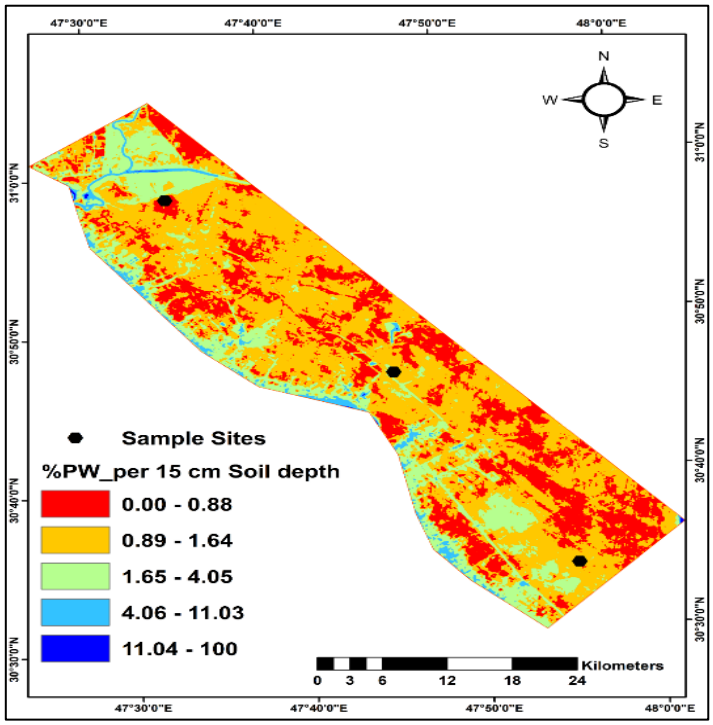

Figure 7. Spatial Distribution of Stored Soil Moisture from Remote Sensing.

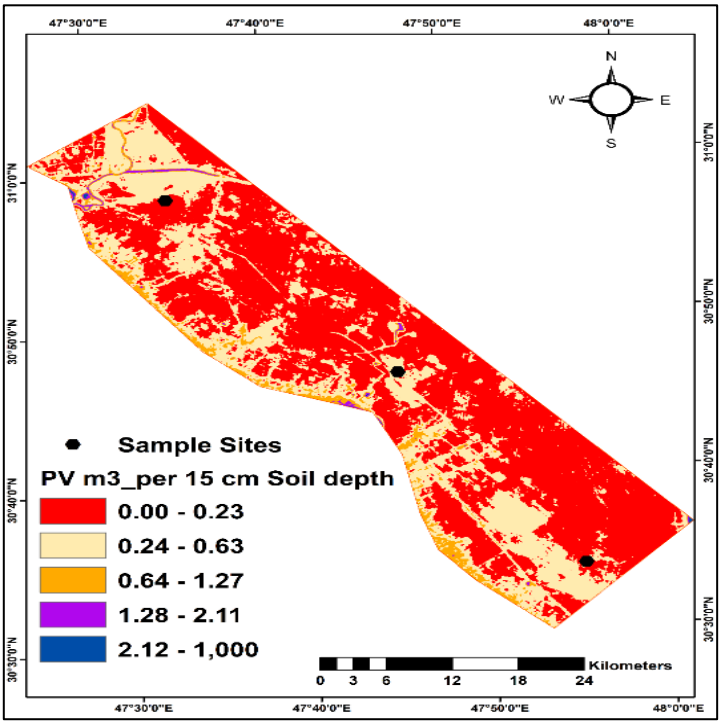

Figure 8. Spatial Distribution of Stored Soil Moisture from Remote Sensing.

Conclusions

- The proposed predictive model is effective in monitoring and estimating the volume of water stored in the soil.
- The use of remote sensing data and satellite imagery is feasible for studying water resources.
- It is evident that areas distant from water sources and with sparse vegetation experience higher temperatures, which has resulted in increased water deficits in the study area.

- The volume of water stored in the soil is higher in areas near water sources due to the impact of lateral water replenishment from the Shatt al-Arab River and its tributaries towards the adjacent soils.

Recommendations

- It is recommended to use geomatics technologies for studying environmental and hydrological variables and monitoring water resource parameters.
- It is advised to apply the proposed model for predicting the volume of water stored in the soil, particularly in arid and semi-arid regions.
- Measures should be taken to mitigate the direct impact of temperatures on the volume of stored water, such as creating a green belt around the remote areas in Basrah Governorate.

References

[1] W. Kinzelbach, P. Brunner, A. von Boetticher, L. Kgotlhang, and C. Milzow, "Sustainable water management in arid and semi-arid regions," in Groundwater Modelling in Arid and Semi-Arid Areas, Cambridge University Press, 2010, pp. 119–130. doi: 10.1017/CBO9780511760280.009.

[2] C. Costanzo, R. Padulano, and T. Caloiero, "Advances in Flow Modeling for Water Resources and Hydrological Engineering," Hydrology, vol. 9, no. 12. MDPI, Dec. 01, 2022. doi: 10.3390/hydrology9120228.

[3] M. C. Anderson, R. G. Allen, A. Morse, and W. P. Kustas, "Use of Landsat thermal imagery in monitoring evapotranspiration and managing water resources," Remote Sens. Environ., vol. 122, pp. 50–65, Jul. 2012, doi: 10.1016/j.rse.2011.08.025.

[4] S. Mallah, B. Delsouz Khaki, N. Davatgar, R. R. Poppiel, and J. A. M. Demattê, "Digital Mapping of Topsoil Texture Classes Using a Hybridized Classical Statistics–Artificial Neural Networks Approach and Relief Data," AgriEngineering, vol. 5, no. 1, pp. 40–64, Mar. 2023, doi: 10.3390/agriengineering5010004.

[5] F. Ming, L. Chen, D. Li, and X. Wei, "Estimation of hydraulic conductivity of saturated frozen soil from the soil freezing characteristic curve," Sci. Total Environ., vol. 698, Jan. 2020, doi: 10.1016/j.scitotenv.2019.134132.

[6] M. S. Malik, J. P. Shukla, and S. Mishra, "Effect of Groundwater Level on Soil Moisture, Soil Temperature and Surface Temperature," J. Indian Soc. Remote Sens., vol. 49, no. 9, pp. 2143–2161, 2021, doi: 10.1007/s12524-021-01379-6.

[7] C. A. Black, D. D. Evans, J. L. White, L. E. Ensminger, F. E. Clark, and R. C. Dinauer, "Methods of soil analysis: Part 1 physical and mineralogical properties, including statistics of measurement and sampling," Am. Soc. Agron. Madison, Wisconsin, USA, pp. 1–770, 1965, doi: 10.1002/9780891182030.

[8] F. M. Howari, M. Sharma, C. M. Xavier, Y. Nazzal, I. Ben Salem, and F. Al Aydaroos, "Remote sensing and GIS based approaches to estimate evapotranspiration in the arid and semi-arid regions," https://doi.org/10.1117/12.2599899, vol. 11856, pp. 85–92, Sep. 2021, doi: 10.1117/12.2599899.

[9] A. Rostami, M. Raeini-Sarjaz, J. Chabokpour, and A. A. Chadee, "Soil moisture monitoring by downscaling of remote sensing products using LST/VI space derived from MODIS products," Water Supply, vol. 23, no. 2, pp. 688–705, Feb. 2023, doi: 10.2166/WS.2023.002.

[10] N. Tajudin, N. Ya'acob, D. M. Ali, and N. A. Adnan, "Soil moisture index estimation from Landsat 8 images for prediction and monitoring landslide occurrences in Ulu Kelang, Selangor, Malaysia," Int. J. Electr. Comput. Eng., vol. 11, no. 3, pp. 2101–2108, Jun. 2021, doi: 10.11591/ijece.v11i3.pp2101-2108.

[11] H. A. Al-Sayaab, "Impact of sunspots on climate and hydrology of Shatt Al-Arab Delta Impact of sunspots on climate and hydrology of Shatt Al-Arab Delta Impact of sunspots on climate and hydrology of Shatt Al-Arab Delta," vol. 10, no. 1, 2014.

[12] M. S. Le and Y. A. Liou, "Spatio-temporal assessment of surface moisture and evapotranspiration variability using remote sensing techniques," Remote Sens., vol. 13, no. 9, 2021, doi: 10.3390/rs13091667.

[13] K. Salman and B. A. Al Razaq, "Monitoring Land Surface Temperature (LST) and Land Cover of Basra Province using Remote Sensing Technique and GIS," Iraqi J. Phys., vol. 21, no. 2, pp. 60–73, 2023, doi: 10.30723/ijp.v21i2.1117.

[14] J. Liu et al., "Visible and near-infrared spectroscopy with chemometrics are able to predict soil physical and chemical properties," J. Soils Sediments, vol. 20, no. 7, pp. 2749–2760, 2020, doi: 10.1007/s11368-020-02623-1.

[15] Z. Zhu, S. Qiu, B. He, and C. Deng, "Cloud and Cloud Shadow Detection for Landsat Images: The Fundamental Basis for Analyzing Landsat Time Series," Remote Sens. Time Ser. Image Process., no. May, pp. 3–23, 2019, doi: 10.1201/9781315166636-1.
[16] E. S. Mohamed, A. Ali, M. El-Shirbeny, K. Abutaleb, and S. M. Shaddad, "Mapping soil moisture and their correlation with crop pattern using remotely sensed data in arid region," Egypt. J. Remote Sens. Sp. Sci., vol. 23, no. 3, pp. 347–353, Dec. 2020, doi: 10.1016/j.ejrs.2019.04.003.
[17] B. Zhang et al., "Impacts of River Bank Filtration on Groundwater Hydrogeochemistry in the Upper of Hutuo River Alluvial Plain, North China," Water (Switzerland), vol. 15, no. 7, 2023, doi: 10.3390/w15071343.
[18] J. J. Nsiah, C. Gyamfi, G. K. Anornu, and S. N. Odai, "Estimating the spatial distribution of evapotranspiration within the Pra River Basin of Ghana," Heliyon, vol. 7, no. 4, 2021, doi: 10.1016/j.heliyon.2021.e06828.